Cantilevered microfiber Bragg Grating sensor with high ultrasonic sensitivity and designable resonant frequency

Hanqi Zhang, Qi Wu, Xiangroug Su, Jun Guo, Ke Xiong, Tong Sun and Kenneth T V Grattan

***Abstract*—A cantilevered microfiber Bragg grating (CMFBG) sensor with high sensitivity and resonant frequency which can be designed as required, has been proposed and demonstrated using experimental, theoretical, and simulation methods. The CMFBG design can have a variable cross-section, and has been created to operate by receiving ultrasonic guided waves through the adhesive used. This allows for the formation of standing waves, when the wave is reflected from the end of the device, and also allows for concentrating the ultrasonic energy using the small fiber diameter that forms the device. Compared to a cantilevered conventional fiber Bragg grating, the CMFBG design proposed demonstrates a significant increase in signal amplitude of 227% for a chirp ultrasonic input and 204% for a pencil lead break input. The device exhibits a detuning phenomenon as its resonant frequency difference differs from that of the standing wave with the cantilevered fiber Bragg grating. In addition, the research carried out has shown that the geometric parameters of the CMFBG design, such as the diameter and the length ratio (between the waist and the taper regions), influence the ultrasonic sensitivity and the resonant frequencies observed.**

***Index Terms*—Optical fiber sensor, Bragg grating, ultrasonics, amplifiers, cantilever beams**

I. Introduction

Ultrasonic detection is receiving considerable interest for use in many applications such as structural health monitoring, quality control, and material testing [1]. However, an ultrasonic signal in a large-scale structure typically propagates over long distances but attenuates significantly, leading to a weak amplitude being detected and poor signal-to-noise ratio [2]. For example, detecting ultrasonic signals in full-size aerospace structures using traditional ultrasonic sensors is challenging [3]. Hence, improving the characteristics of ultrasonic devices is a crucial requirement for better sensing performance.

Traditional ultrasonic sensors are usually made from lead-zirconate-titanate (PZT) [4], and can be divided into 'broadband' and 'resonant' types, according to their response characteristics [5]. The broadband sensor is advantageous for detecting signals from sources with unknown frequencies, ensuring that the bandwidth covers the frequencies that are likely to occur and be detected [6]. In contrast, the resonant sensor usually has a higher sensitivity than the broadband sensor around its resonant frequencies and thus is suitable for the detection of signals of pre-determined frequency. For example, resonant sensors can be applied to acousto-ultrasonic detection, which gives the desired input signal to these structures [7]. However, PZT has some drawbacks for routine use, such as large bulk size and sensitivity to stray electromagnetic interference, hindering its performance in practical applications [8]. The Fiber Bragg Grating (FBG) is an alternative approach as the basis of an effective ultrasonic sensor, as it does not show the drawbacks inherent with the PZT [9], [10]. However, the ultrasonic sensing performance of a normal FBG is insufficiently high to allow for the detection of weak signals.

A range of different methods have been proposed to improve the ultrasonic sensitivity of the FBG. For example, phase-shifted FBGs (PSFBGs) have been proposed as the basis of a high-sensitivity broadband sensor [11], [12]. The sharp slope of their performance characteristics and the narrow full width at half maximum seen cause a limited dynamic range, which then requires a high-performance demodulation technique to compensate for even a small degree of environmental fluctuation, such as is caused by temperature excursions and static strain. A similar trade-off between the dynamic range and the sensitivity is also found in superstructured gratings [13]. To tackle this limitation in the system optical design, a microfiber Bragg grating (MFBG) has been proposed, taking advantage of the mechanics of the device [14] where the MFBG amplifies the ultrasonic signal by gathering the ultrasonic energy using the small diameter of the fiber. This provides a simple way to improve the sensitivity, while retaining the high dynamic range of a normal FBG.

In addition to these broadband FBG sensors, several types of resonant FBG sensors have also been studied, such as the cantilevered FBG (CFBG) [15], [16]. As one end of the CFBG is fixed and the other end is free, this creates a short cantilever beam, where the direct wave and the reflected wave can

This work was supported by the National Key R&D Program of China (2021YFF0501800), National Natural Science Foundation of China (11972016, 12111530106), Grant of State Key Laboratory of Mechanics and Control of Mechanical Structures (MCMS-I-0521G04), a Project Funded by the Priority Academic Program Development of Jiangsu Higher Education Institutions, and the Royal Society (IEC\NSFC\201414) (*Corresponding authors: Qi Wu*)

Hanqi Zhang, Qi Wu, Xiangroug Su, Jun Guo, and Ke Xiong are with the State Key Laboratory of Mechanics and Control for Aerospace Structures, Nanjing University of Aeronautics and Astronautics, No. 29 Yudao Street, Nanjing 210016, China (e-mail: hanqi_zhang@nuaa.edu.cn; wu.qi@nuaa.edu.cn; sx2201138@nuaa.edu.cn; junguo@nuaa.edu.cn; kxiong@nuaa.edu.cn).

Tong Sun and Kenneth T V Grattan are with the School of Science & Technology, City, University of London, Northampton Square, London EC1V 0HB, United Kingdom (e-mail: t.sun@city.ac.uk; k.t.v.grattan@city.ac.uk).

interfere with each other in the cantilever beam and thus can form a standing wave. Subsequently, the magnitude exhibits a marked augmentation around the resonant frequency of the standing wave. However, the CFBG has limited sensitivity adjustability and relies only on the length of the beam to determine the resonant frequency, posing difficulties in further improving the sensitivity or achieving a desired resonant frequency, and consequently hindering the overall sensing performance of the sensor. Hence, there is a crucial need to develop a new and effective FBG-based resonant sensor to enhance the sensing performance and control both the sensitivity and resonant frequency.

In this study, a new design of a cantilevered microfiber Bragg grating (CMFBG) sensor is proposed and discussed. The sensor has a high sensing performance in the ultrasonic domain, where the key sensing characteristics (including sensitivity and resonant frequency) can be controlled by appropriate design of the geometric parameters of the system. To illustrate this best, this paper is organized as follows: Section II introduces the manufacturing method and experiments on the CMFBG; Section III provides a theoretical and simulation verification, and the effects of the geometric features of the design on sensitivity and the resonant frequency are described in Section IV. Finally, the key conclusions of the work are presented in Section V.

II. Experiment

A. Design of CMFBG

The CMFBG used in this study was fabricated from a 'normal' FBG using a recently developed chemical etching method [17]. The diameter of FBG was then 125 μm, after removing the coating, and the grating length was 5 mm. A part of the optical fiber (with a length of 10.5 mm where the grating had been written) was etched using a 5 mol/L NaOH solution in a hydrothermal reactor, which was placed into a high-temperature test chamber. The maximum temperature of the chemical etching process was set at 120 ℃, and the holding time in it was controlled, with the aim of achieving the desired diameter of the CMFBG. As shown in Fig. 1(a), the spectrum of the CMFBG is not distorted, and the corresponding slope of the linear region is 6.18 nm^{-1}, approximating to the initial value of 6.39 nm^{-1}. Fig. 1(b) shows such a CMFBG, with in this case a diameter of 35 μm. The cantilever beam of the CMFBG includes a part of the pigtail (with a length of 2 mm), a taper region (with a length of 2.25 mm), and a waist region (with a length of 8.25 mm). Unlike the common cantilevered measurement method, in which the length of the cantilever beam is literally infinite [14], the cantilever beam of the CMFBG considered is short as, in this experiment, the length was only 12.5 mm. In the work described in the following, CMFBGs with diameters of 35 μm are referred to as a '35 μm CMFBG', the diameter of the CMFBG is described by D, and the length of the taper region and waist region are termed L_t and L_w, respectively.

Fig. 1(c) shows the schematic diagram of the ultrasonic sensing approach using the CMFBG developed above. The ultrasonic wave propagates from the adhesive (shown in red on the figure) into the optical fiber and thus transfers into a longitudinal and transverse wave, propagating through the cantilever beam with no dispersion as optical fiber can be regarded as a string-like waveguide [5]. The wave is then reflected from the end of the waist region and passes through the cantilever beam again. The direct and reflected waves shown in the figure, with the same frequency and opposing direction continuously traverse between the fixed and free ends, resulting in the formation of a standing wave. Differing from the normal standing wave of the CFBG, the standing wave propagating in the CMFBG is amplified and detuned, a feature which will be investigated later.

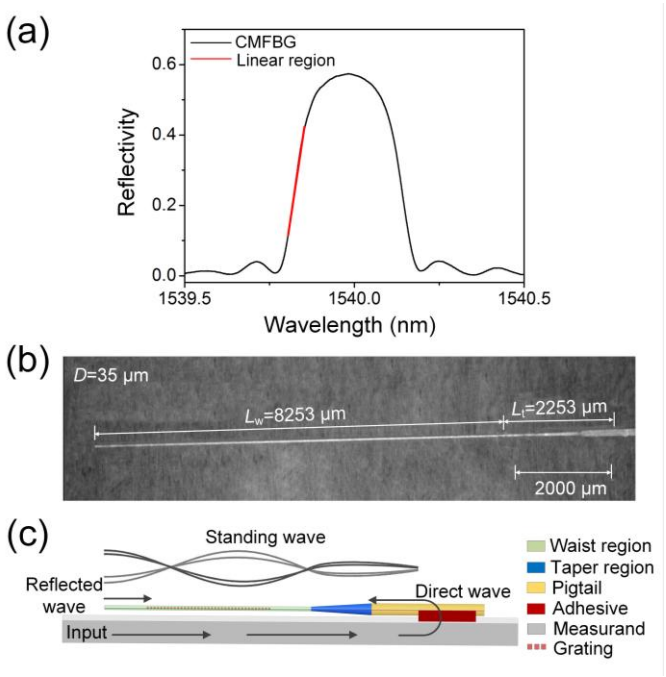

Fig. 1. Schematics of the CMFBG set up used (a) Spectrum of the CMFBG. (b) Microphotography of the CMFBG (with diameter of 35 μm). (c) Illustration of the ultrasonic wave propagating in the cantilever beam and the standing wave.

B. Experimental setup

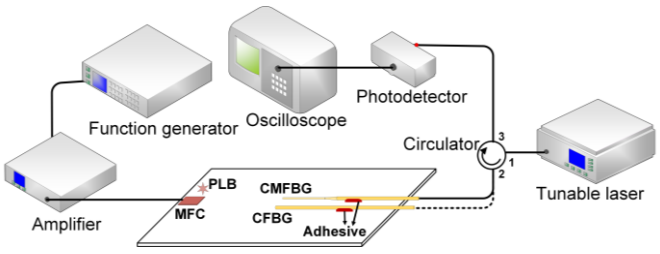

Fig. 2. Ultrasonic system for comparison of CMFBG and CFBG when the input was excited by MFC and PLB.

The acousto-ultrasonic test was conducted on an aluminum plate with dimensions of 250 × 250 × 1 (L × W × H) mm^3, this being used to demonstrate the characteristics of the CMFBG, by comparing the performance to a 'normal' FBG, as shown in Fig. 2. The excitation system of acousto-ultrasonic test contains a function generator (Agilent 33521A), a power amplifier (Aigtek, ATA-43151), and a macro fiber composite (MFC)

(Smart Material, M-0714-P2) sensor [18]. The function generator generated a chirp signal, the frequency of which was swept from 10 to 1000 kHz (over a time of 0.1 ms) with a peak-to-peak voltage of 10 V [19]. Then, the signal was amplified (by 6 times) using the power amplifier and it was input into the aluminum plate through the MFC. The distance between the excitation and the adhesive point of CMFBG was 100 mm. In addition, a pencil lead break (PLB) test, which is known as a Hsu-Nielsen source [20], was also performed to investigate the potential of the CMFBG in acoustic emission test. A 2-mm length pencil lead was broken on the surface of the aluminum plate to induce a simulated acoustic emission signal with a small energy.

The CMFBG sensing system output was demodulated using the edge filter method [10]. A tunable laser signal (Santec, TSL710, with an output power of 3 dBm) was used to illuminate the system. The wavelength of the laser was locked at the 3 dB position in the linear region of the CMFBG. This position has the highest slope, and thus a slight wavelength shift induced by the ultrasonic signal can cause a significant change in the reflected optical power. The optical power was then output to the photodetector (Thorlabs, PDA10CS2) and converted to a voltage signal, which is recorded using an oscilloscope (Keysight, DSOX2004A). In addition, the signals from a reference CFBG were also demodulated, using the same setup.

C. Experimental Results

Figs. 3(a) and (b) show the waveforms and the corresponding spectra detected by the CMFBG and CFBG in the acousto-ultrasonic test. The waveform received by the CMFBG was significantly higher in amplitude than that of the CFBG. The peak amplitudes of the received CMFBG and CFBG waveforms were 37.6 and 11.5 mV, indicating that the CMFBG showed a 227% increase over that for the CFBG. The amplitude of the CMFBG received signal was also obviously higher than that of the CFBG received signal in the frequency domain. The signal-to-noise ratios of the signals received by the CMFBG and CFBG were 41.8 and 36.3 dB, respectively. The first three resonant frequencies of the CMFBG are 150, 399, and 491 kHz, and those of the CFBG are 105, 311, and 510 kHz. Unlike the regular resonant frequency of the CFBG, the resonant frequency of the CMFBG does not increase in simple multiples, indicating a detuning resonant phenomenon is occurring. Hence, the experimental result indicates that the ultrasonic sensitivity of CMFBG was remarkably improved, compared with what was seen from the CFBG. Moreover, the detuned resonant frequency of the CMFBG could be observed, the characteristics of which can be specifically designed by controlling the geometric parameters of the setup (as will be discussed in detail below). The PLB test was repeated more than three times, and all the results indicate that the CMFBG is superior to the CFBG in terms of sensitivity. Fig. 3(c) and (d) present a typical result of the PLB test. The peak amplitudes of PLB signal received by the CMFBG and CFBG are 42.2 and 13.9 mV, suggesting that the CMFBG shows a 204% increase compared to the CFBG. Therefore, the CMFBG also has an outstanding ultrasonic sensing performance seen in the PLB test, illustrating its potential to be applied to acoustic emission.

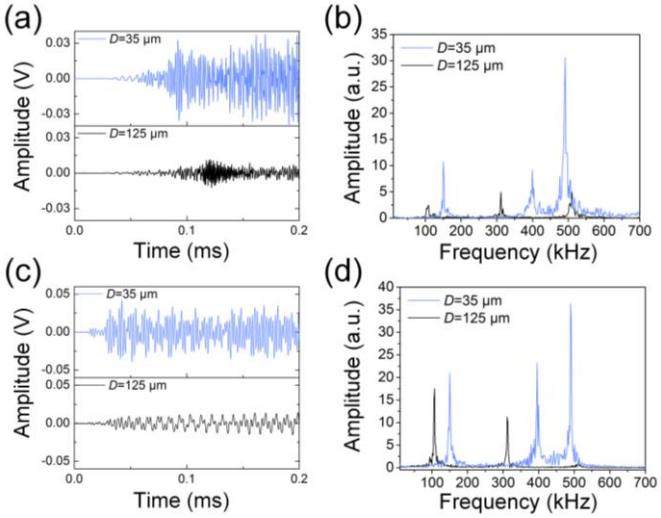

Fig. 3. Ultrasonic signals received by the CMFBG and CFBG in the time domain excited by (a) the MFC and (b) the corresponding spectra obtained and (c) the PLB and (d) the corresponding spectra obtained.

Furthermore, the ultrasonic sensitivity of the sensor is evaluated. In the cantilever structure, the Bragg wavelength shift $\Delta\lambda_S$ is proportional to the input strain ε, given as,

$$\Delta\lambda_S = aA\varepsilon \tag{1}$$

where a is a strain sensitivity of a conventional FBG with a value of 1.2 pm/με, and A is the amplification factor representing the ratio of input and output strains of the cantilever structure. As it is well known that the voltage of an ultrasonic signal is proportional to the strain [14], A can be written as,

$$A = V_{output} / V_{input} \tag{2}$$

where V_{output} is the peak amplitude of the detected signal by the CMFBG or CFBG, and V_{input} is the peak amplitude of the detected signal when an FBG is directly glued at the adhesive point of the structure, which is demonstrated as 5.7 mV in an experiment. Therefore, A is calculated as 6.60 and 2.02 for the CMFBG and CFBG, respectively. The amplitude of an ultrasonic signal V_S is given as [12],

$$V_S = GR_D Pg\Delta\lambda_S \tag{3}$$

where R_D is the response factor of the photodetector with a value of 1.4 V/mW; G is the grating slope, P is the input laser power, and g is the gain setting of the amplifier, the values of these three parameters can be found in the above sections. The minimum detectable strain $\varepsilon_{\min}$, is defined as the strain that causes V_S with the same peak amplitude of noise V_N. Substituting equation (1) into (3) yields

$$\varepsilon_{\min} = \frac{V_N}{aAGR_D Pg} \tag{4}$$

where V_N of the CMFBG or CFBG shows the same value of 0.028 mV because of the same demodulation system used. Substituting the values of parameters into equation (4) yields $\varepsilon_{\min}$ that is 0.20 nε and 0.65 nε to CMFBG and CFBG,

respectively. Hence, the CMFBG exhibits a higher sensitivity than the CFBG.

III. Theoretical and Simulation Verification

A. Ultrasonic theory of CMFBG

The ultrasonic resonant frequency of the CMFBG can be theoretically described by using the ultrasonic transfer matrix method, an approach which establishes the relationship between the ultrasonic input and the output of the acoustic structure using the matrix [21]. The CMFBG can be regarded as a three-section acoustic structure composed of two uniform cross-section structures (namely the waist region and the pigtail of the CMFBG) and a conical structure (namely the taper region of the CMFBG). The ultrasonic input and output of the CMFBG can be expressed by the transfer matrix as follows,

$$\begin{bmatrix} p_{output} \\ v_{output} \end{bmatrix} = [T_3][T_2][T_1] \begin{bmatrix} p_{input} \\ v_{input} \end{bmatrix} \quad (5)$$

where p is the sound pressure, v is the particle velocity, and the subscripts *input* and *output* indicate the input and output values, respectively. $[T_3]$, $[T_2]$, and $[T_1]$ are the ultrasonic transfer matrices of the waist region, taper region, and pigtail, respectively. Then, the sound pressure level (SPL) transfer function H can be defined as shown below where,

$$H = 20\lg\left|\frac{p_{output}}{p_{input}}\right| \quad (6)$$

Fig. 4 shows the illustration of H of the 35 μm CMFBG introduced in Section II calculated by inputting the geometric parameters of the set up into equation (5) and (6). Also, the H value of the CFBG was calculated. The frequencies corresponding to the peak value of H indicate the resonant frequencies of the sensor. Thus, the first three theoretical resonant frequencies of the CMFBG were 146, 394, and 496 kHz, and those of the CFBG were 106, 317, and 528 kHz. The theoretical resonant frequency of the CFBG increases in clear multiples, fitting well to fundamental vibration differential equations [5]. Compared to the CFBG (whose resonant frequency depends only on the length of the cantilever beam), the resonant frequency of the CMFBG was influenced by multiple parameters and can be controlled more flexibly.

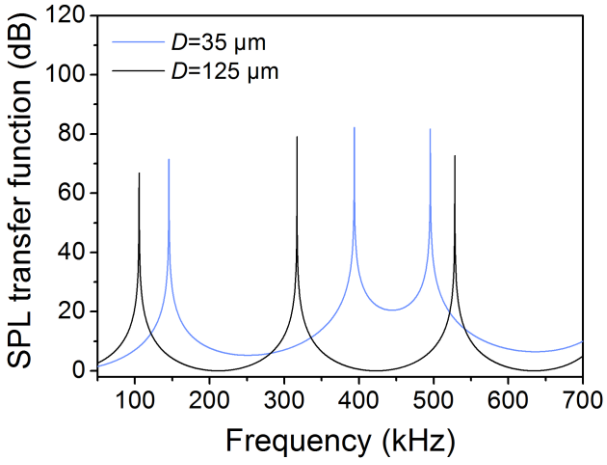

Fig. 4. SPL transfer function of the 35 μm CMFBG and CFBG.

B. Ultrasonic simulation of CMFBG

The finite element method (FEM) was also employed in the work carried out to investigate the sensing performance of the CMFBG, by using LS-DYNA software. In the FEM model shown in Fig. 5, the aluminum plate was simulated having dimensions of 25 ×2 ×1 (L ×W ×H) mm^3 (these being chosen to shorten the calculation time needed). The geometrical parameters of the CMFBG model were the same as those of the CMFBG used in the experiment carried out. The adhesive region used was 5 mm in length, where this connects the aluminum plate and the pigtail. In addition, the boundary conditions of the plate and the end of the pigtail were set to be non-reflective (referenced to the actual dimension of the plate and pigtail of the CMFBG). The material properties used were taken from data published [22]. The input signal was the same chirp signal as in the experiment, and was loaded at the position marked in the figure. In addition, a model of the CFBG was also simulated and results compared.

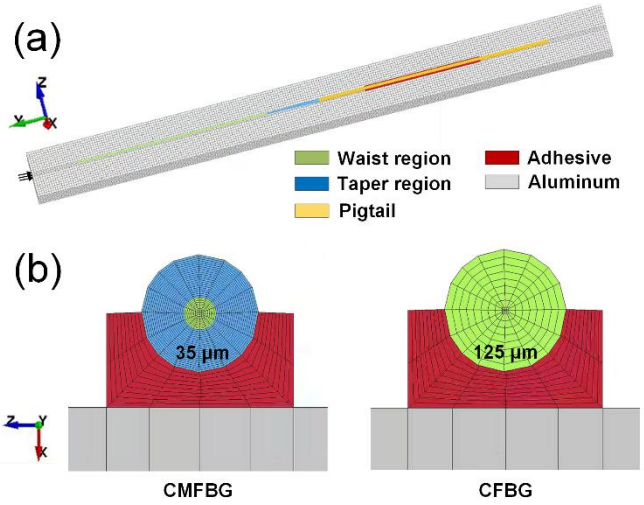

Fig. 5. (a) Diagram of the parameters of the finite element model. (b) Models of the CMFBG and the CFBG used.

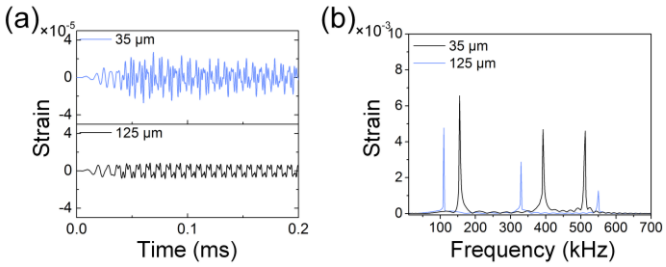

Fig. 6. Simulated signals received by the CMFBG and the CFBG (a) in the time domain and (b) in the frequency domain.

Fig. 6(a) shows the results of the simulation of the CMFBG and the CFBG, extracted from the neural axis of the waist region (as our previous study demonstrated that the axial strain of the elements on the neural axis of the optical fiber model represents the key response of the sensor [14]). The waveforms are not closely similar to those seen from the experimental

results because of the shortened simulated propagation distance, the frequency characteristics of the actuator, and the adhesive conditions, where it is difficult for these to be completely consistent with the experiment. However, given that, the simulated ultrasonic sensing performance of the CMFBG and the CFBG agrees well with the experimental results. The received waveform at the CMFBG has a higher amplitude than the received signal at the CFBG, suggesting the superior ultrasonic sensitivity of the CMFBG. Fig. 6(b) presents the results of the simulation in the frequency domain where the amplitude of the CMFBG is also higher than that of the CFBG in the frequency domain. The first three simulated frequencies of the CMFBG were 156, 393, and 513 kHz, and those of the CFBG were 110, 330, and 550 kHz. The different resonant characteristics of the CMFBG and the CFBG used were clearly observed in the simulation results.

C. Comparison of the Characteristics

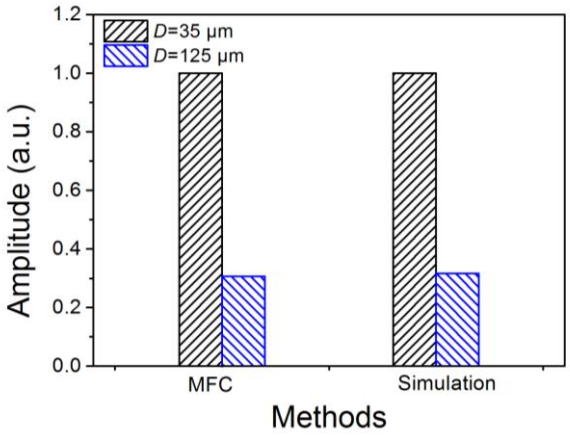

Fig. 7. Comparison of signal amplitudes obtained by the acousto-ultrasonic test and simulation.

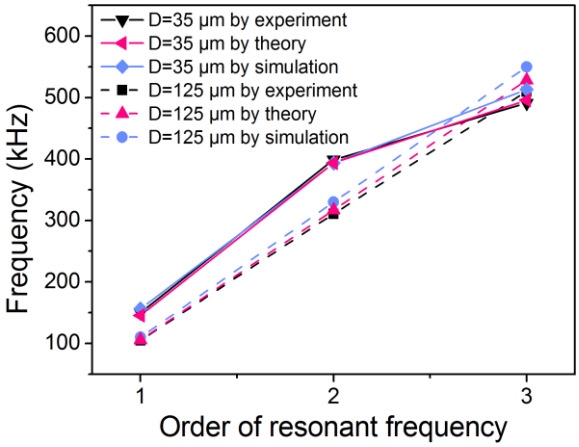

Fig. 8. Comparison of resonant frequency obtained by the acousto-ultrasonic test, theory and simulation.

Fig. 7 shows the peak amplitudes of the ultrasonic signals in the time domain extracted from the experimental and simulation results obtained. The amplitudes were normalized with reference to the amplitude of CMFBG for a better comparison and exhibits similar results. Fig. 8 shows the first three resonant frequencies extracted from the experimental, theoretical, and simulation results obtained. It is clear from the results obtained that the experimental resonant frequencies were consistent with the theoretical and simulation resonant frequencies, as the errors between the results of the experiment and the other two methods were less than 4.6% and 7.9%, respectively. This high level of agreement indicates the reliability of the results. Finally, the sensitivity and the resonant frequency of the CMFBG were further investigated, with a view to enhance the design of the sensor.

IV. Discussion of Geometric Parameters

A. Ultrasonic sensitivity

The geometry of CMFBG was mainly determined by the parameters D and L_w/L_t. Tables 1 and 2 display the parameters (of the variable D and L_w/L_t) of the CMFBG, respectively. Table 1 includes 6 models, in which the diameter increases from 20 to 125 μm. L_w and L_t used in the models were 2.25 and 8.25 mm, thus L_w/L_t was 3.67, except for Model 6. Here Model 6 has a diameter of 125 μm, corresponding to the normal CFBG, which does not have a taper region. Table 2 contains 5 models, in which L_w and L_t change from 6.25 to 10.25 mm and from 4.25 to 0.25 mm, respectively. The corresponding values of L_w/L_t in the models vary from 1.47 to 41 and the diameter used in the models was 35 μm. In particular, the total length of the waist region and the taper region remained at 10.5 mm, and the length of the cantilever beam was fixed at 12.5 mm in these models. The ultrasonic sensing characteristics of the CMFBG (with varying values of D and L_w/L_t) were investigated only by introducing these parameters in Tables 1 and 2 into the simulation methods, as the reliability of the simulation has been verified in Section III.

TABLE 1
VARIABLE D FOR THE CMFBG

Parameter	Model					
	1	2	3	4	5	6
L_t (mm)	2.25	2.25	2.25	2.25	2.25	0
L_w (mm)	8.25	8.25	8.25	8.25	8.25	10.5
D (μm)	20	30	35	40	50	125

TABLE 2
VARIABLE L_W/L_T FOR THE CMFBG

Parameter	Model				
	1	2	3	4	5
L_t (mm)	4.25	3.25	2.25	1.25	0.25
L_w (mm)	6.25	7.25	8.25	9.25	10.25
L_w/L_t	1.47	2.23	3.67	7.4	41
D (μm)	35	35	35	35	35

Fig. 9 shows the simulation results achieved when varying D and L_w/L_t in the time domain. The waveforms decrease with the increase of the value of D, however, there is no clear trend seen in the waveforms as L_w/L_t varies. Fig. 10(a) shows the normalized peak amplitude when the value of D increases,

which has a linear downward trend with the slope of -0.0066 and R^2 of 0.93. Thus, the ultrasonic sensitivity of the CMFBG can be linearly controlled by adjusting the value of D. Fig. 10(b) shows the normalized peak amplitude when the value of L_w/L_t increases. Although the peak amplitude shifts irregularly with the change of L_w/L_t, the maximum difference in the peak amplitude is only 27.7%. Hence, the influence of L_w/L_t is negligible, illustrated when designing the ultrasonic sensitivity of the CMFBG, as this effect is much smaller than that due to the change in the value of D.

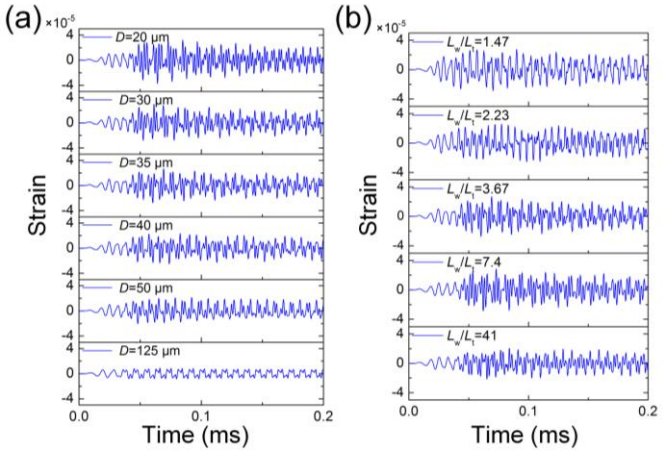

Fig. 9. Simulation results of CMFBG in the time domain when the (a) D increases from 20 μm to 125 μm and (b) L_w/L_t increases from 1.47 to 41.

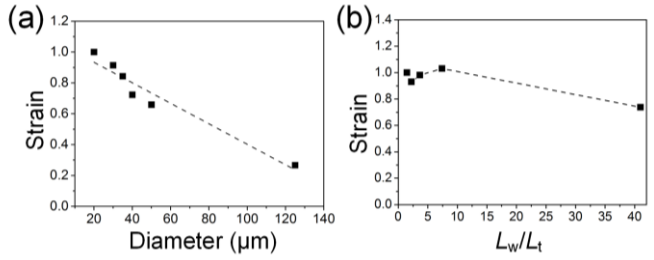

Fig. 10. Peak amplitude of simulation waveforms when the (a) D increases from 20 μm to 125 μm and (b) L_w/L_t increases from 1.47 to 41.

B. Resonant frequency

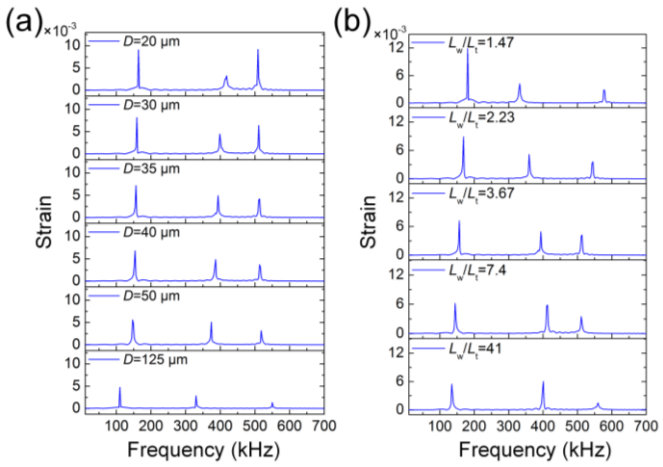

Fig. 11. Simulation results for the CMFBG in the frequency domain when the (a) D increases from 20 μm to 125 μm and (b) L_w/L_t increases from 1.47 to 41.

The simulation results achieved when varying D and L_w/L_t in the frequency domain are shown in Fig. 11. The shift of the resonant frequency with the changing values of D and L_w/L_t can be clearly observed. The solid lines in Fig. 12(a) show the first three resonant frequencies of CMFBG when the value of D increases. The linear fitting was carried out and the slopes of the first three resonant frequencies were -0.513, -0.762, and 0.407, and the corresponding R^2 values were 0.99, 0.93, and 0.99, respectively. The solid lines in Fig. 12(b) show the first three resonant frequencies of the CMFBG when the value of L_w/L_t varies, which changes dramatically before the value of L_w/L_t of 7.4, and then becomes stable when the value of L_w/L_t reaches 7.4.

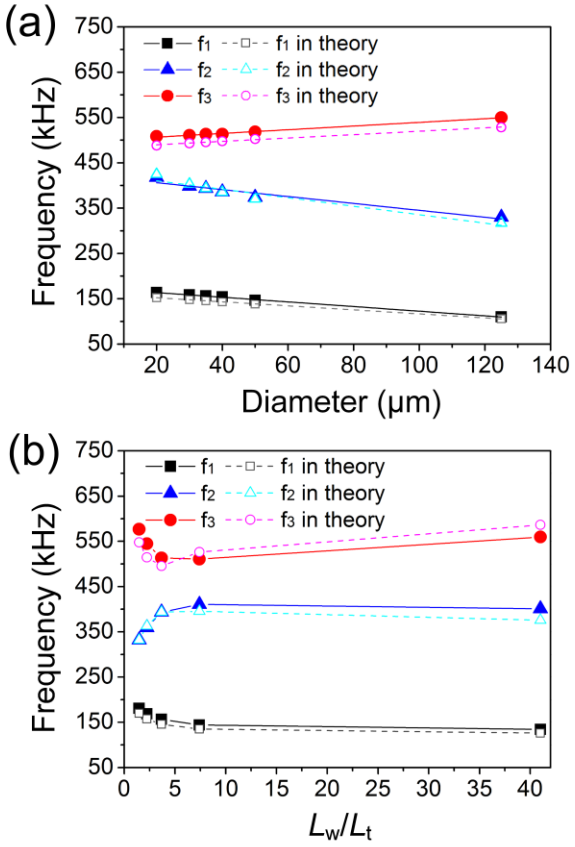

Fig. 12. Simulation and theoretical resonant frequencies seen when the (a) D increases from 20 μm to 125 μm and (b) L_w/L_t increases from 1.47 to 41.

The theoretical resonant frequency is also calculated. The dashed lines in Fig. 12(a) show the theoretical resonant frequency for the situation where D increases, which is highly consistent with the results of the simulation resonant frequency, with an error being below 7.0%. The slopes of the linear fitting of the theoretical results were -0.443, -0.936, and 0.373, and the corresponding R^2 values were 0.99, 0.92, and 0.99, which are similar to the simulation results. Hence, the theoretical and simulation analysis illustrates that the resonant frequency of the CMFBG was linearly related to the value of D, and therefore, the resonant frequency can be designed precisely in the sensor by adjusting the value of D. The dashed lines in Fig. 12(b)

present the theoretical resonant frequency seen when L_w/L_t increases, this being in good agreement with the resonant frequency seen from the simulation. The error between the theoretical and simulation frequency is less than 6.9%. Therefore, both the simulation and the theoretical analysis reveal that even a small change in the value of L_w/L_t can result in an evident shift in the resonant frequency of the CMFBG, that is, the resonant frequency can be effectively controlled by adjusting the value of L_w/L_t in the sensor, when L_w/L_t is less than 7.4.

V. Conclusion

In this study, a CMFBG sensor consisting of variable cross-section optical fiber has been proposed and demonstrated. The signal amplitude obtained from a 35 μm CMFBG, which was manufactured through the chemical etching method, showed a remarkable increase of 227% and 204% in the acousto-ultrasonic and PLB tests, respectively, when compared to the CFBG. This is due to the small diameter concentrating the ultrasonic energy and the resonant characteristics demonstrated further improving the device sensitivity. The CMFBG shows a detuning phenomenon with the first three resonant frequencies of 150, 399, and 491 kHz, which are different from the resonant frequencies of 105, 311, and 510 kHz of the CFBG. Then, a theoretical analysis using the transfer matrix method and simulation analysis using the FEM method were conducted to verify the experimental results. The experimental frequency shows errors lower than 4.6% and 7.9%, compared to the theoretical and simulation results, respectively. Moreover, the results of the investigation reveal that D was linearly related to the ultrasonic sensitivity of the CMFBG, and both the D and L_w/L_t values affect the resonant frequency of the CMFBG.

Compared to existing resonant sensors like the CFBG, the bridged FBG, and the capsular FBG, as well as compared to the MFBG, the proposed CMFBG retains two advantages of higher sensitivity and detuning resonant frequency simultaneously. This outstanding ultrasonic sensing performance and the flexibility in the design of the resonant frequency allow the CMFBG used to have the potential for a large number of practical applications, especially for the detection of low-amplitude and frequency-determined signals. In addition, suitable encapsulation technology can be implemented on the CMFBG to protect the sensor from the environmental fluctuations [16]. It is our view that by replacing the FBG with a PSFBG within the CMFBG, the sensitivity of the sensor could be further improved. However, the diameter of the CMFBG taper region in this study is simplified, using a linear decrease in the design. Other profile shapes (such as an exponential or a hyperbolic profile) may have different ultrasonic sensing characteristics, and these will be investigated in the future studies that are underway.

References

[1] Q. Wu, Y. Okabe, and F. Yu, "Ultrasonic structural health monitoring using fiber Bragg grating," *Sensors.*, vol. 18, no. 10, Oct, 2018, Art. no. 3395.

[2] M. Gresil and V. Giurgiutiu, "Prediction of attenuated guided waves propagation in carbon fiber composites using Rayleigh damping model," *J. Intell. Mater. Syst. Struct*., vol. 26, no. 16, pp. 2151–2169, Sep. 2015.

[3] H. Zhang, T. Liu, J. Lu, R. Lin, C. Chen, Z. He, S. Cui, Z. Liu, X. Wang, B. Liu, K. Xiong, Q. Wu, "Static and ultrasonic structural health monitoring of full-size aerospace multi-function capsule using FBG strain arrays and PSFBG acoustic emission sensors," *Opt Fiber Technol*., vol. 78, Jul. 2023, Art. no. 103316.

[4] J. F. Tressler, S. Alkoy, and R. E. Newnham, "Piezoelectric sensors and sensor materials," *J. Electroceram*., vol. 2, pp. 257-272, Mar.1998.

[5] J. R. Lee and H. M. Jeong, "Design of resonant acoustic sensors using fiber Bragg gratings," *Meas. Sci. Technol*., vol. 21, no. 5, Mar. 2010, Art. no. 057001.

[6] P. J. de Groot, P. A. M. Wijnen, and R. B. F. Janssen, "Real-time frequency determination of acoustic emission for different fracture mechanisms in carbon/epoxy composites," *Compos Sci Technol*., vol. 55, no. 4, pp. 405–412, Aug. 1955.

[7] S. H. Lim, I. K. Oh, and J. R. Lee, "Ultrasonic active fiber sensor based on pulse-echo method." *J. Intell. Mater. Syst. Struct*., vol. 20, no, 9, pp. 1035–1043, Jun. 2009.

[8] R. Wang, Q. Wu, K. Xiong, J. Ji, H. Zhang, and H. Zhai, "Phase-shifted fiber Bragg grating sensing network and its ultrasonic sensing application," *IEEE Sens. J*., vol. 19, no. 21, pp. 9790–9797, Nov, 2019.

[9] G. Wild and S. Hinckley, "Acousto-ultrasonic optical fiber sensors: overview and state-of-the-art," *IEEE Sens. J*., vol. 8, no. 7, pp. 1184–1193, Jul. 2008.

[10] G. Wild, S. Hinckley, and P. V. Jansz, "A transmit reflect detection system for fiber Bragg grating photonic sensors," *Proc. SPIE*., vol. 6801, 2007, Art. no. 68010N.

[11] Q. Wu, Y. Okabe, K. Saito, and F. Yu, "Sensitivity distribution properties of a phase-shifted fiber Bragg grating sensor to ultrasonic waves," *Sensors*., vol. 14. no. 1, pp. 1094–1105, Jan. 2014.

[12] Q. Wu and Y. Okabe, "High-sensitivity ultrasonic phase-shifted fiber Bragg grating balanced sensing system," *Opt. Exp.*, vol. 20, no. 27, pp. 28353–28362, Dec. 2012.

[13] A. I. Azmi, D. Sen, W. Sheng, J. Canning, and G. D. Peng, "Performance enhancement of vibration sensing employing multiple phase-shifted fiber Bragg grating," *J. Lightwave Technol*., vol. 29, pp. 3453–3460, Nov. 2011.

[14] H. Zhang, H. Zhu, Q. Wu, Y. Chen, R. Wang, F. Xu, and K. Xiong, "Microfiber Bragg grating bonded using tapered cantilever for high-sensitivity ultrasonic detection," *J. Lightwave Technol*., vol. 41, no. 1, pp. 355–361, Jan. 2023.

[15] H. Tsuda, E. Sato, T. Nakajima, H. Nakamura, T. Arakawa, H. Shiono, M. Minato, H. Kurabayashi, and A. Sato, "Acoustic emission measurement using a strain-insensitive fiber Bragg grating sensor under varying load conditions," *Opt. Lett.*, vol. 34, no. 19, pp. 2942–2944, Oct. 2009.

[16] H. Zhang, Q. Wu, C. Chen, Z. Liu, T. Bai, and K. Xiong, "Porosity evaluation of composites using the encapsulated cantilever fiber Bragg grating based acousto-ultrasonic method," *IEEE Sens. J*., vol. 22, no. 16, pp. 15991–15998, Aug. 2022.

[17] K. J. Zhu, J. Guo, Q. Wu, X. R. Wu, Z. Zhang, P. D. Zhang, Y. Rao, and P. H. Liang, "A batch preparation method of microfiber grating sensors," CN. Patent 202211292340.7, Oct. 1, 2022.

[18] Macro Fiber Composite (MFC) Brochure. Accessed: Nov. 23, 2021. [Online]. Available: https:// www.smart-material.com.

[19] J. E. Michaels, S. J. Lee, A. J. Croxford, and P. D. Wilcox, "Chirp excitation of ultrasonic guided waves," *Ultrasonics*., vol. 53, pp. 265–270, Jul. 2013.

[20] A. Mostafapour, M. Ghareaghaji, S. Davoodi, and A. Ebrahimpour, "Theoretical analysis of plate vibration due to acoustic signals," *Applied Acoustics*, vol. 103, pp. 82–89, Feb. 2016.

[21] Q. Min, Q. Y. Zhang, J. J. Tian, Q. B. Wang, and W.Q. He, "A study on the dissonant standing-wave tube with variable section and its extremely nonlinear standing-wave field," *Phys. Lett. A*., vol. 377, no. 1–2, pp. 99–106, Nov. 2012.

[22] F. Yu, Y. Okabe, Q. Wu, and N. Shigeta, "Fiber-optic sensor-based remote acoustic emission measurement of composites," *Smart Mater. Struct*., vol. 25, no. 10, Sep. 2016, Art. no. 105033.